Indonesian Geotechnical Journal, August 2026, Vol 5 (2). Page 89-106
DOI: https://doi.org/10.56144/igj.v5i2.154
EISSN: 2589-7520
https://indonesian-geotechnical-journal.org/index.php/JGI/issue/archive

Effectiveness of Spider Web Foundation Versus Raft Foundation in Resisting Static and Dynamic Loads at Liquefaction Prone Area

Abram Kris Wicaksono[1,*], Martin Wijaya[1], Paulus P. Rahardjo[1]
[1]Department of Civil Engineering, Faculty of Engineering, Universitas Katolik Parahyangan, Bandung, Indonesia 40141
*Correspondence: abramkw@gmail.com

SUBMITTED 9 April 2026 **REVISED** 30 August 2026 **ACCEPTED** 31 August 2026

ABSTRACT As one of the earthquake-prone countries with liquefaction risk in certain soil conditions, Indonesia has developed innovative earthquake-resistant infrastructure. One of the innovations is Konstruksi Sarang Laba-Laba foundation (KSLL), literally translated as spider web foundation. The KSLL foundation system was invented by Ir. Sutjipto and Ir. Riyantori in 1976. This research compares the KSLL foundation against the conventional raft foundation in resisting static and dynamic loads. The study was based on data from University Hospital in Jember which uses KSLL as its foundation. Based on the soil investigation data, a water-saturated loose sandy soil, which is suspected to have liquefaction potential, was identified at a depth of 5-9 m. Based on liquefaction potential assessment, the study site has a high liquefaction potential with an LPI value of 27.7. Finite Element Method was used to compare the KSLL foundation against a raft foundation with equal concrete volume to the KSLL foundation. The results indicate that the KSLL foundation performs better than the equivalent raft foundation, having lower settlement under both static and dynamic loading conditions. Although higher axial forces were observed in the KSLL foundation, its overall performance remained superior. In contrast, the equivalent raft foundation developed high bending moments and shear forces, experiencing localized punching deformation. These findings demonstrate that the KSLL foundation provides a more effective foundation for structures constructed on liquefaction-prone ground by enhancing stability and reducing deformation.

KEYWORDS KSLL Foundation; Spider Web Foundation; Raft Foundation; Finite Element Modelling; Dynamic Analysis; Liquefaction

1 INTRODUCTION

Of the various potential natural disasters that can occur in Indonesia, earthquakes are one of the most dangerous natural disasters for the construction of a building. Earthquakes can cause both upper structure and lower structure failures in the form of building foundations. In addition, with certain soil conditions, earthquakes can also trigger one of the dangerous natural disasters, namely liquefaction.

With these concerns, in 1976, Ir Sutjipto and Ir. Ryantori from the Institu Teknologi Sepuluh Nopember (ITS) created and patented (by PT. Katama Suryabumi) a foundation design called Konstruksi Sarang Laba-Laba (KSLL), literally translated as Spider Web Construct. Figure 1 shows a photograph of KSLL foundation system. It is considered as shallow foundation constructed using upright ribs arranged like a spider web. Its arrangement led to an earthquake efficient design, using minimum volume of concrete, but capable of achieving high dynamic load resistance.

This study aims to compare the effectiveness of KSLL foundations versus conventional raft foundation in receiving earthquake loads. Three-dimensional finite element method was used for the analysis. A case study of a university hospital constructed using KSLL foundation in Jember was used as the basis of analysis.

Figure 2 shows the KSLL foundation layout for the university hospital. The University Hospital is located on Slamet Riyadi Street, Patrang, Jember, East Java. It consists of 4 floors + 1 roof floor.

The base of the foundation is located at a depth of 3 meters below the existing ground surface. The KSLL foundation concrete ribs were casted using K-225 concrete quality. There are two types of ribs with different dimensions, namely RIB P with a rectangular cross section dimension of 100 x 900 mm and RIB K with a rectangular cross section dimension of 120 x 1300 mm (Figure 2). The spaces between the ribs are filled with compacted sand and then covered with 14 cm thick concrete plate of K-225 concrete quality.

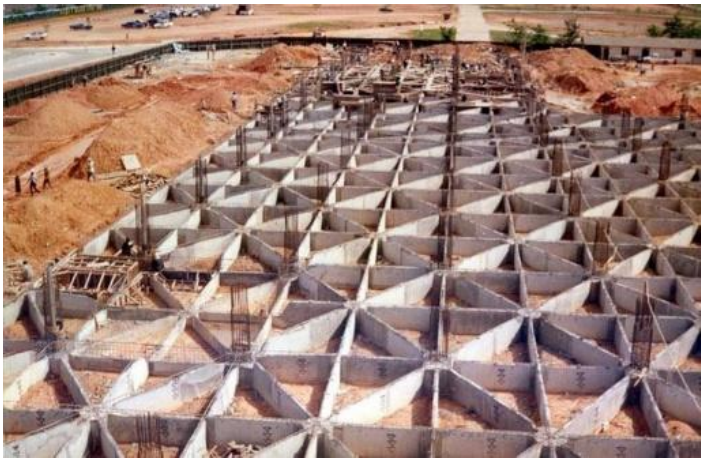

Figure 1. Illustration of KSLL / Spider Web Foundation (PT Katama Suryabumi, 2011)

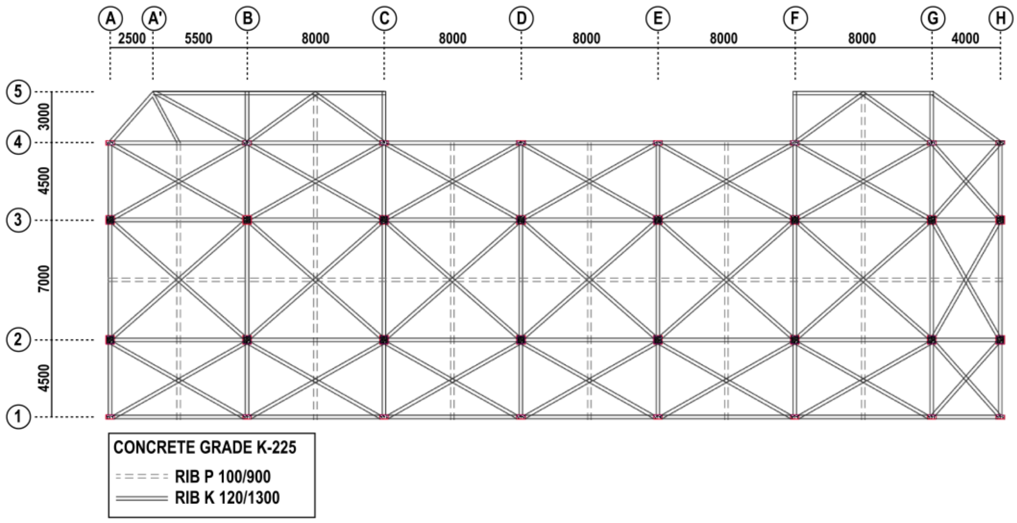

Figure 2. KSLL foundation configuration of University Hospital in Jember

2 GEOTECHNICAL INVESTIGATION

Figure 3 shows the boring log and SPT data for one of the boreholes conducted at the project site. The groundwater table is found 1.5 m below the ground surface. The first layer (topsoil) is brown colored silt, followed by brown sand with dense consistency (average NSPT of 42). The third layer consist of blackish brown sand with loose consistency (average NSPT of 8). The fourth layer consist of blackish brown sand with medium dense consistency (average NSPT of 19). The fifth layer is blackish brown sand with dense consistency (average NSPT of 38). The last layer is blackish brown sand with a very dense consistency (NSPT > 60).

Based on the site investigation, a loose, groundwater-saturated sand layer was identified between depths of approximately 5 to 9 m, with SPT N-values ranging from 5 to 11. Grain-size analyses (see Section 3.3) indicate that the soil consists predominantly of clean to slightly gravelly sand with low fines content and falls within the range of potentially liquefiable soils. Combined with the loose density condition, these characteristics suggest a high liquefaction susceptibility for the layer.

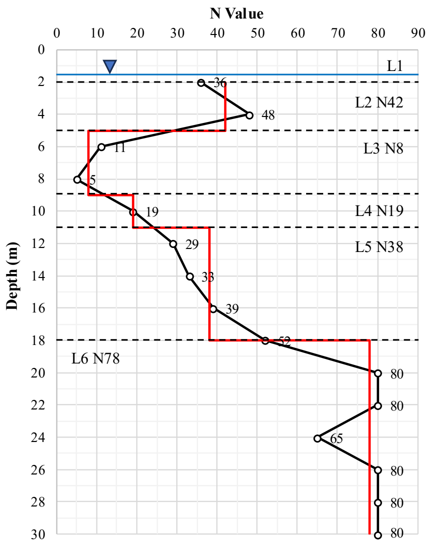

Layer ID	Depth [m]	N-Value	Soil Description	Soil Color
L1	0	-	Clayey SILT	Brown
L2	2	36	Dense SAND with trace silt and trace gravel	
	4	48		
L3	6	11	Loose SAND with gravel	Blackish Brown
	8	5		
L4	10	19	Medium dense SAND with gravel	
L5	12	29	Dense SAND with gravel	
	14	33		
	16	39		
	18	52		
L6	20	80	Very dense silty SAND	
	22	80		
	24	65		
	26	80		
	28	80		
	30	80		

Figure 3. SPT Result and Soil Stratification

3 LIQUEFACTION ASSESSMENT

Liquefaction phenomenon is defined as the transformation of granular soil layers from solid to liquid-like due to an increase in pore water pressure and a decrease in effective stress (Marcuson, 1978). The increase in pore water pressure occurs due to the tendency of granular soil to compact under dynamic loads (earthquake). To determine liquefaction potential, there are several criteria that need to be identified, namely historical criteria, geological criteria, and compositional criteria. After the three criteria have been, the results are used to review the liquefaction potential in said location. Liquefaction potential index (LPI) and safety factor can then be calculated.

3.1 Historical Criteria

Earthquake records as historical evidence can be used and collected to determine historical criteria at a location with suspected liquefaction potential as shown in Figure 3. Ambraseys (1988) combined data from earthquake magnitude data with epicentral distances at locations that have experienced liquefaction to obtain limits related to estimating the criteria for a location with liquefaction potential. In his research, Ambraseys (1988) estimated the epicentral distance limit of historical earthquake data to the review location as far as 500 km with a minimum earthquake magnitude of 5. The collection and grouping of earthquake data with magnitude (M) > 5 was carried out in the period 1924-2024 at a radius of 500 km to the University Hospital in Jember. The historical earthquake catalogue contains several events that plot above the Ambraseys (1988) boundary curve, indicating that the study area has experienced seismic events with sufficient magnitude and proximity to satisfy the historical criterion for liquefaction susceptibility.

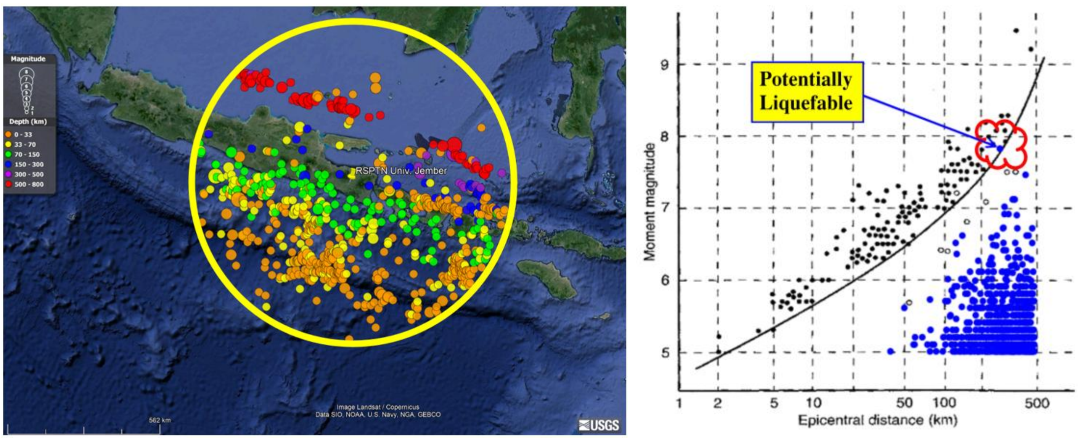

Figure 3. Historical criteria at study case area (USGS and Ambraseys, 1988)

3.2 Geological Criteria

Based on the Geological Map of Jember Java Sheet (KemenESDM RI, Figure 4a), the building is in the Qvab and Qvat formations. Qvab formation is Argopuro Breccia formation, and Qvat formation is Argoputro Tuff formation. From this information, it is known that the soil conditions at this location are volcanic materials consisting of andesite-structured breccia deposits and lava inserts and tuff materials (tuff, lithic tuff, ash tuff, and vitric tuff). Site investigation data indicate the presence of sandy soil layers below the groundwater table, which is located approximately 1.5 m beneath the ground surface. Volcanic deposits may weather into granular soils that can become susceptible to liquefaction under favorable conditions.

3.3 Composition Criteria

One of the criteria for liquefaction is based on the grain size gradation composition of soil material. Tsuchida (1970) proposed a curve containing the limits of grain size distribution of soil with liquefaction potential. At the study area, grain size distribution tests were conducted on the samples collected from the boring. To focus on the layer identified as potentially liquefiable from the SPT profile, together with one layer above and one layer below, selected grain-size distribution curves were plotted against the Tsuchida (1970) boundaries, as shown in (Figure 4b).

The results indicate that several samples, particularly those obtained from the loose sand layer between depths of approximately 5 and 10 m (SPT N-values ranging from 5 to 11), fall within or near the potentially liquefiable zone proposed by Tsuchida (1970). The samples from 5.5-6 m and 7.5-8 m depth, which correspond to the lowest SPT N-values, show the closest agreement with the liquefiable soil boundaries. Although some samples partially extend beyond the recommended range, the overall gradation characteristics of the loose sandy layer are consistent with soils commonly associated with liquefaction susceptibility. These observations support the subsequent liquefaction assessment based on the NCEER procedure and Liquefaction Potential Index (LPI) analysis.

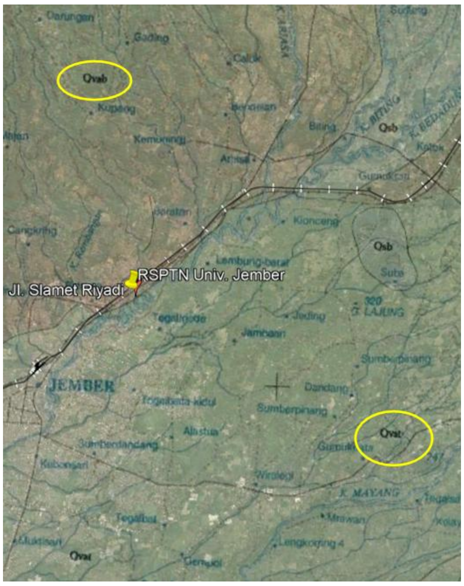

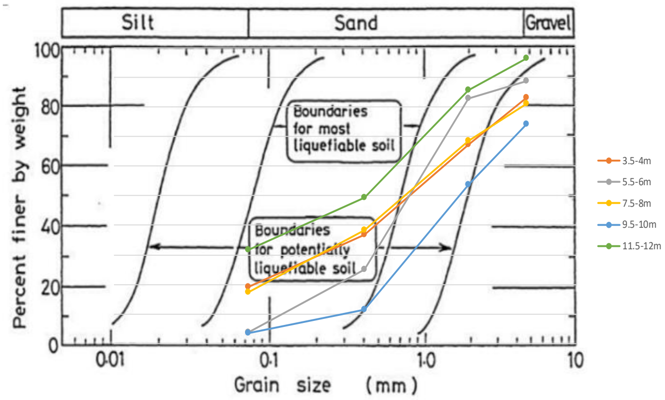

a) b)

Figure 4. a) Geological criteria (KemenESDM RI) and b) Composition criteria (Tsuchida, 1970) at study case area

3.4 Safety Factor and Liquefaction Potential Index

To determine and identify layers that have liquefaction potential, a liquefaction potential assessment was conducted using the NCEER (1998) method from Youd and Idriss (2001). The PGA value for Jember City was taken as 0.4g (Design Spektra Indonesia, PUPR RI, 2019). Figure 5 shows the calculation results. It reveals that at depth 5 to 10 m, the factor of safety is below 1 (CSR > CRR), so this layer has potential to experience liquefaction. The resulting Liquefaction Potential Index (LPI) value is 27.7 and can be categorized as area with high liquefaction potential (very high, major, high).

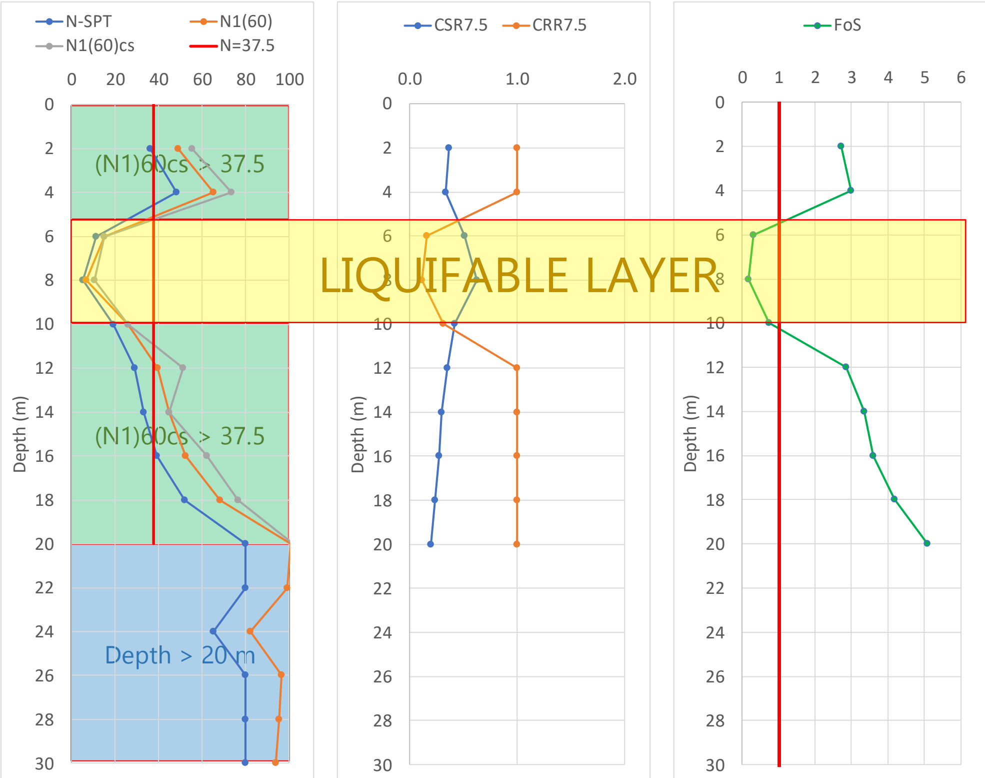

Figure 5. Liquefaction potential analysis at study case area

4 NUMERICAL ANALYSIS MODELLING

The comparative analysis of raft foundation against KSLL foundation under earthquake load was conducted using finite element software, Midas GTS-NX.

4.1 Ground Motion

Dynamic analysis requires a representative earthquake time-history record as input motion. In this study, the input ground motion was adopted from a previous seismic hazard assessment conducted for the University Hospital project in Jember by the co-authors of this study. The seismic hazard assessment included Probabilistic Seismic Hazard Analysis (PSHA), deaggregation analysis, and spectral matching procedures to develop a site-specific earthquake record for a return period of 2475 years.

The deaggregation analysis identified a dominant earthquake scenario with a magnitude of 6.1, hypocentral distance of approximately 70 km, and focal depth of 34 km. Based on these characteristics, the recorded ground motion from the 12 September 2020 Ofunato, Japan earthquake was selected as the seed motion. The record was subsequently modified through spectral matching to be consistent with the target response spectrum obtained from the seismic hazard analysis.

1. Seed motion: 58km SE of Ofunato, Japan 2020-09-12 02:44:11 UTC
2. Magnitude: 6.1
3. Depth: 34 km
4. Hypocenter distance 70 km

The resulting spectrally matched acceleration time history, shown in Figure 6, was used as the seismic input motion for the dynamic finite element analysis performed in this study.

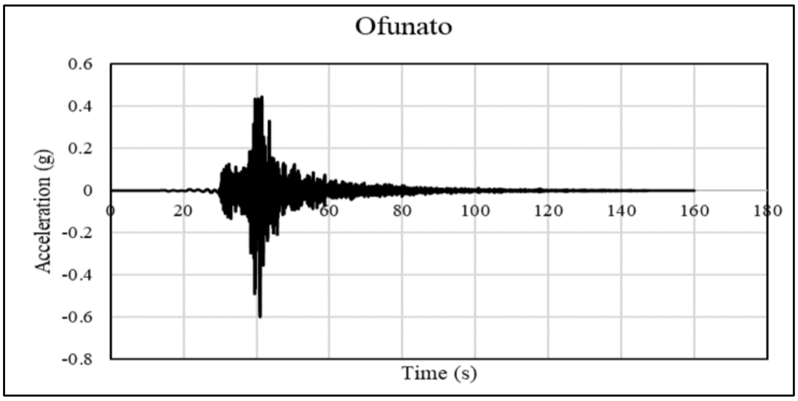

Figure 6. Spectrally matched input ground motion adopted from the site-specific seismic hazard assessment conducted for study case area

4.2 Foundation Modelling

Figure 7 shows the finite element model used for analysis. On the top right is the 3D view of the KSLL foundation, top view of the foundation was also shown in Figure 1b. The foundation was modelled as plate elements with a modulus of 2.03 x 10^7 kPa (also in Table 1 – Concrete Grade K225). The KSLL foundation consists of approximately 64 primary ribs (RIB K, 120 mm × 1300 mm) and 25 secondary ribs (RIB P, 100 mm × 900 mm) arranged in a spider-web configuration. The spaces between the ribs are filled with compacted sand (modelled using layer 1 sand) and covered by a 140 mm thick concrete slab. The cover of the KSLL foundation was not modelled. In total, the KSLL foundation uses 266 m^3 of concrete. This is equivalent to a raft foundation with thickness of 0.29 m.

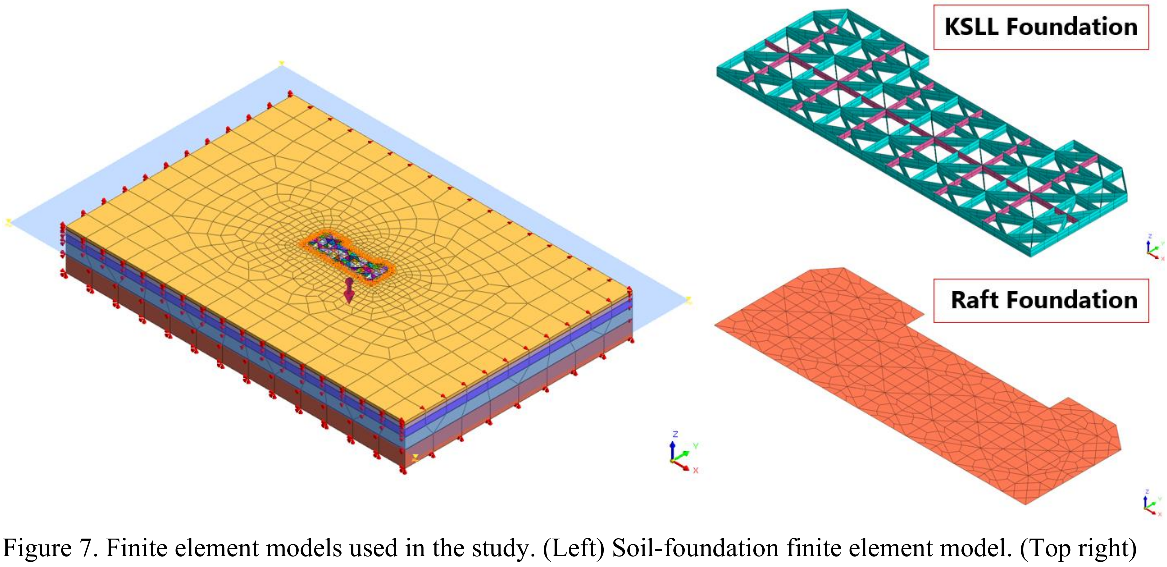

Figure 7. Finite element models used in the study. (Left) Soil-foundation finite element model. (Top right) KSLL foundation model showing RIB P elements (cyan) and RIB K elements (magenta). (Bottom right, orange) Equivalent raft foundation model with the same concrete volume as the KSLL foundation.

4.3 Soil Parameters

Table 1 shows the soil parameters used for analysis. With the exception of layer 3, the constitutive model used for all layers were Mohr-Coulomb.

Table 1. Parameters used in Numerical Analysis

Parameters	Concrete K225	Layer 1 Silt	Layer 2 Sand	Layer 3 Sand (Liq)	Layer 4 Sand	Layer 5 Sand	Units
Depth	-	0-2	2-5	5-10	10-18	18-30	[m]
N-value	-	-	42	12	38	> 60	-
Soil model	Elastic	MC	MC	UBC Sand	MC	MC	-
Drainage Type	Non-porous	Undrained A	Drained	Undrained A	Drained	Drained	-
E	2.03 10^7	5000.0	27291.6	12768.0	25496.1	44289.0	[kN/m^2]
υ’	0.15	0.30	0.30	0.30	0.30	0.30	-
γ	24.00	18.00	18.50	14.00	19.00	20.00	[kN/m^3]
γ_{sat}	-	19.00	19.50	15.00	20.00	21.00	[kN/m^2]
c’	-	1.00	0.00	0.00	0.00	0.00	[kN/m^2]
ϕ’	-	27.00	36.00	see Table 2	35.00	40.00	[°]

* Based on drilling and SPT Data.

For liquefiable layer 3, the constitutive model used was the Modified UBCSAND model. The additional parameters required for the UBCSAND are listed in Table 2. The equations used to estimate the peak friction angle (φ_p), elastic shear modulus (K_G^e), plastic shear modulus (K_G^e) and cap bulk modulus (K_B^e) are taken from Beaty and Byrne (2011) and are shown in Equation 1 to 4.

Table 2. UBC Sand Parameters

Parameters		Units	Default value	Values used
Constant Volume Friction Angle	ϕ_{cv}	[°]	-	8
Peak Friction Angle	ϕ_p	[°]	-	29.76
Cohesion	c	[kN/m^2]	-	0
Elastic Shear Modulus	K_G^e	-	-	1090.57
Plastic Shear Modulus	K_G^p	-	-	923.65
Cap Bulk Modulus	K_B^e	-	-	763.4
Elastic Shear Modulus Exponent	ne	-	0.5	0.5
Plastic Shear Modulus Exponent	np	-	0.5	0.5
Plastic Cap Modulus Exponent	mp	-	0.5	0.5
Failure Ratio	R_f	-	0.9	0.9
Post Liquefaction Calibration Factor	F_{post}	-	0.01	0.01
Soil Densification Calibration Factor	F_{dense}	-	1	1

$$\varphi_p = \varphi_{cv} + \frac{(N_1)_{60}}{10} + \max\left(0; \frac{(N_1)_{60} - 15}{5}\right) \tag{1}$$

$$K_G^e = 21.7 \times 20 \times (N_1)_{60}^{0.3333} \tag{2}$$

$$K_G^p = K_G^e \times (N_1)_{60}^2 \times 0.003 + 100 \tag{3}$$

$$K_B^e = 0.7 \times K_G^e \tag{4}$$

Where $(N_1)_{60}$ is the normalized SPT N-value.

5 ANALYSIS RESULTS

5.1 Deformation under Static Condition

The construction of KSLL foundation and equivalent raft foundation was done in four construction stages: Initial stage, in which the initial stresses are generated; Excavate the foundation area by 3.0 m depth; Installation of KSLL foundation or the equivalent raft foundation; Column loads activation (loads are shown in Figure 8).

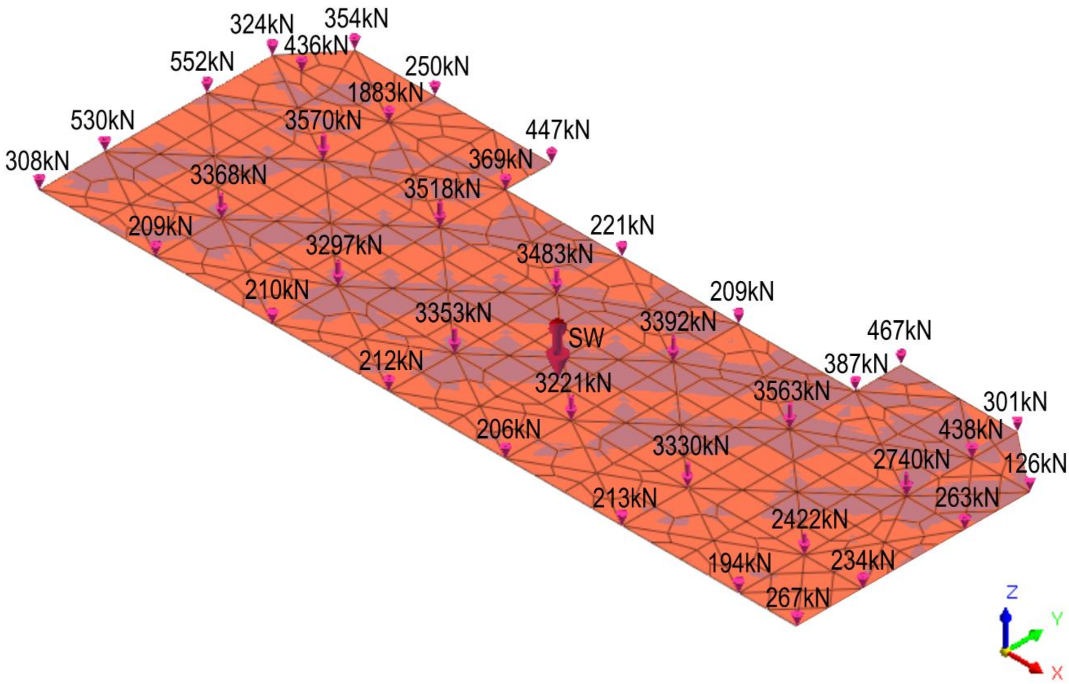

Figure 8. Column loading details

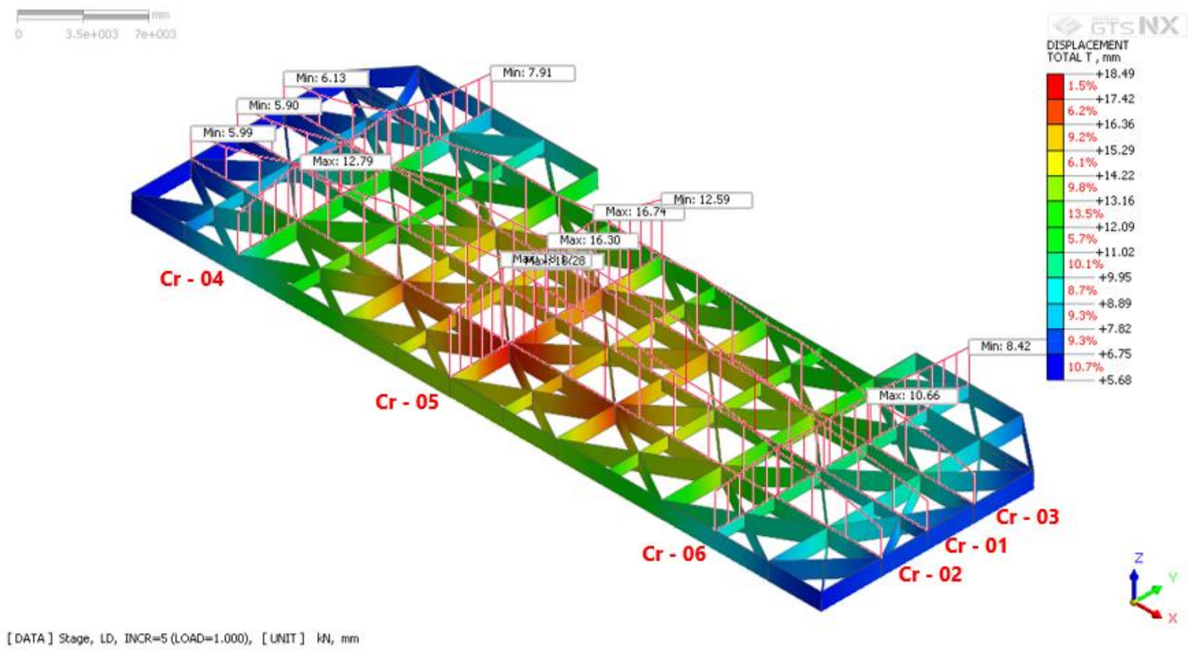

Figure 9. Displacement contour of KSLL Foundation (Static Condition)

The deformation contours for the KSLL foundation and raft foundation are shown in Figure 9 and Figure 10 while the cross-sectional deformation diagrams for both foundations are shown in Figure 11. The maximum settlement of the KSLL foundation is 18.5 mm, smaller than the raft foundation which has a maximum settlement of 32.61 mm.

The raft foundation exhibits a tendency toward local deformation, particularly near the column locations. This behavior indicates stress concentration and insufficient slab stiffness when its thickness is constrained by the volume limitations of the equivalent concrete. In contrast, the KSLL foundation exhibits a more uniform settlement pattern, reflecting a more effective load redistribution mechanism and higher system stiffness.

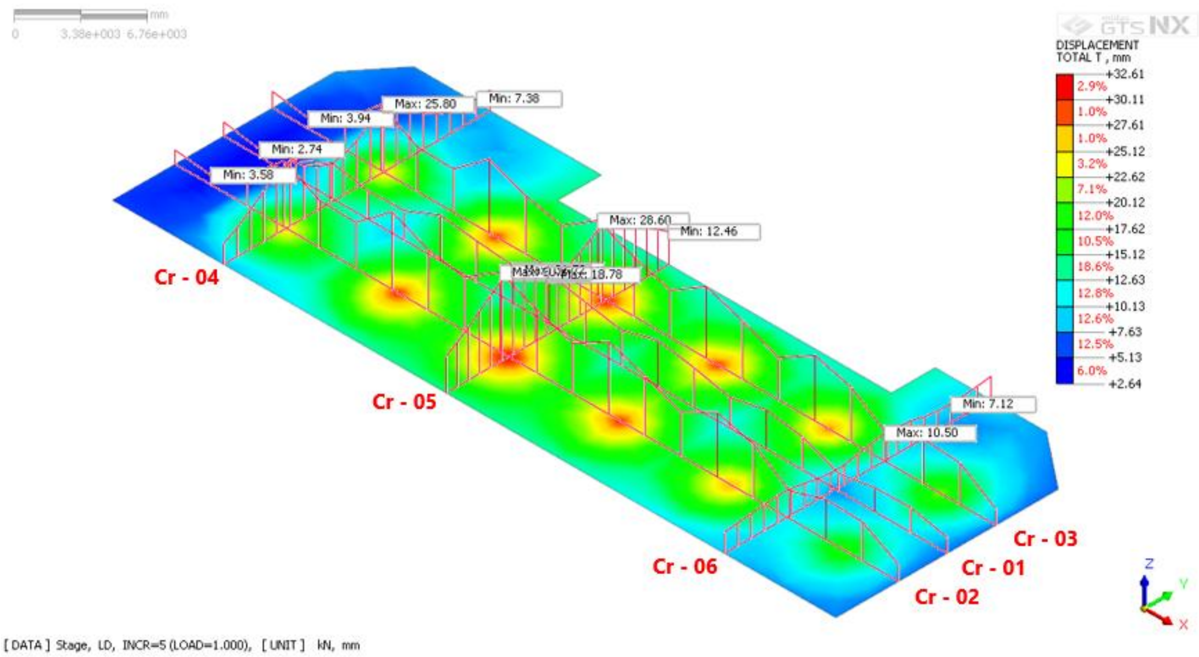

Figure 10. Displacement contour of raft foundation (static condition)

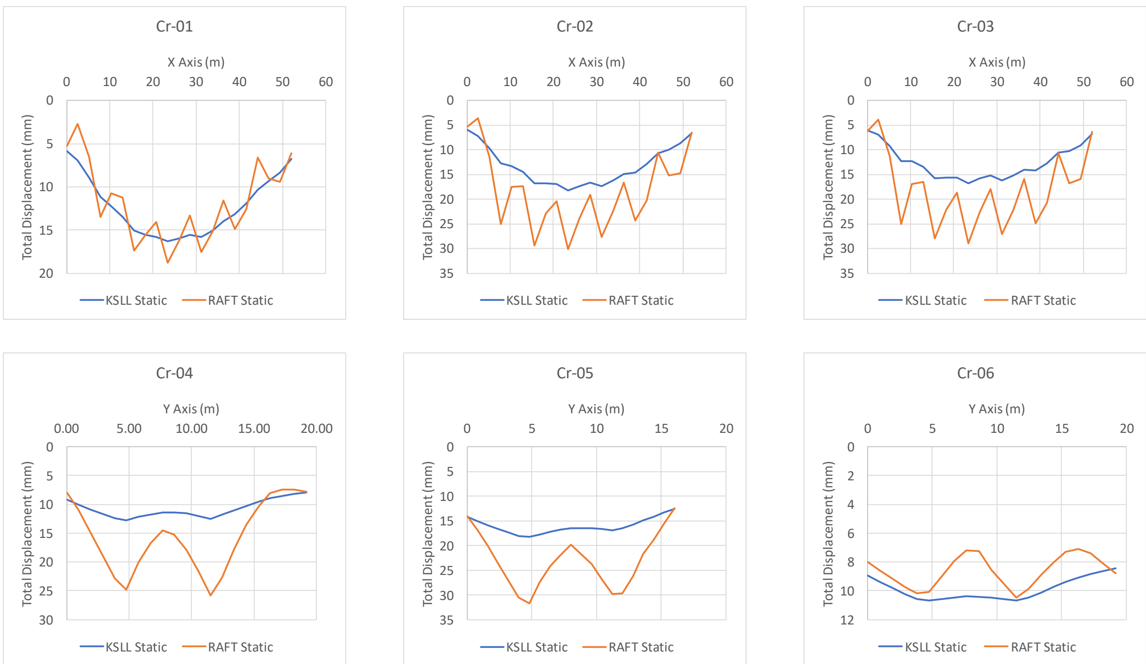

Figure 11. Displacement Diagram of Foundation (Static Condition)

5.2 Deformation on Dynamic Condition

The dynamic condition analysis was conducted using non-linear time history analysis. To simulate liquefaction behaviour during earthquake loading, the liquefable layer identified between depths of 5 and 10 m was modelled using the UBCSand constitutive model. Figure 12 shows the distribution of excess pore water pressure generated during the dynamic analysis. Excess pore pressure developed primarily within the UBCSand layer (blue layer with generated excess pore pressure), whereas the surrounding soil layers modelled using the Mohr-Coulomb constitutive model generated negligible excess pore pressure. This response confirms that the liquefiable soil layer experienced a reduction in effective stress during cyclic loading and contributed to the observed post-earthquake settlements.

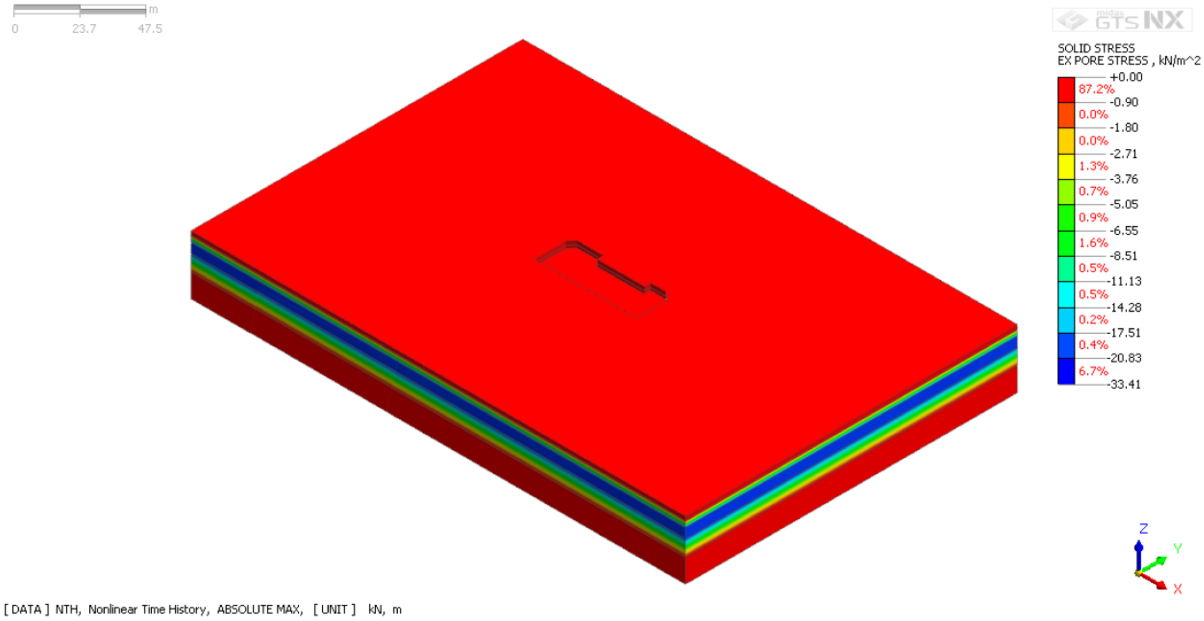

Figure 12. Excess pore water pressure generated during dynamic loading

The maximum excess pore water pressure generated within the liquefiable layer reached approximately 66.8 kPa beneath the central portion of the foundation as shown in Figure 13. The concentration of excess pore pressure within the UBCSand layer demonstrates that the liquefaction mechanism was successfully captured in the numerical model.

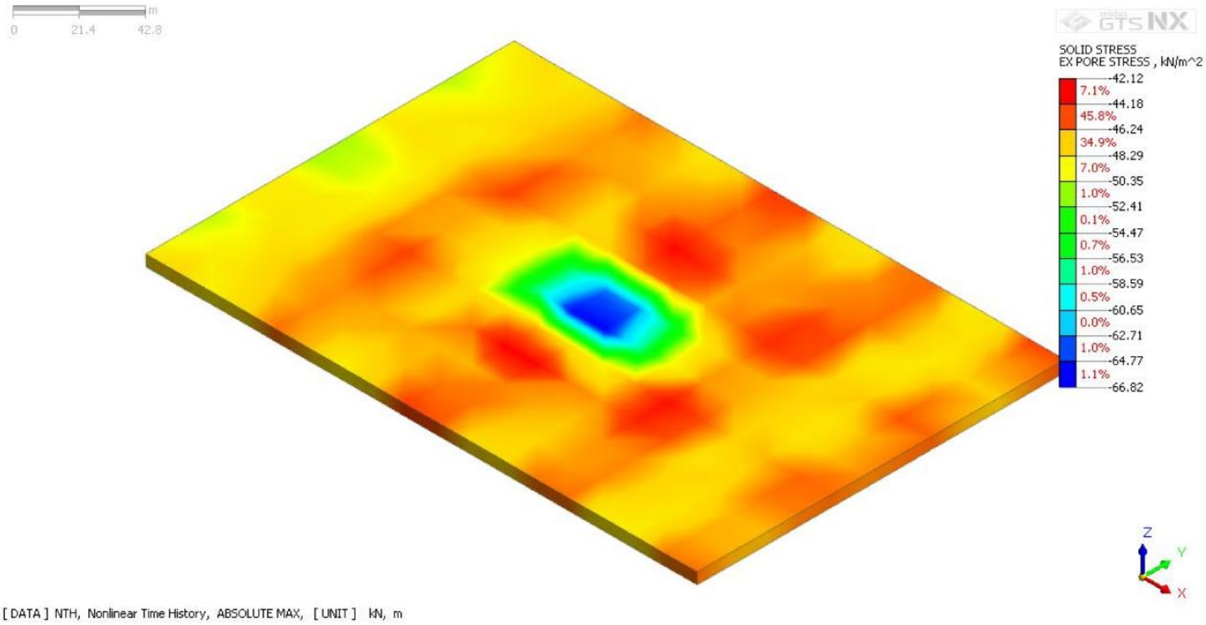

Figure 13. Maximum excess pore water pressure on liquefiable layer generated during dynamic loading

The deformation contours for the KSLL foundation and equivalent raft foundation are shown in Figure 12 and Figure 13 while the cross-sectional deformation diagrams for both foundations are shown in Figure 16. The maximum settlement of the KSLL foundation is 31 mm while the equivalent raft foundation settles more, (maximum displacement = 39.3 mm).

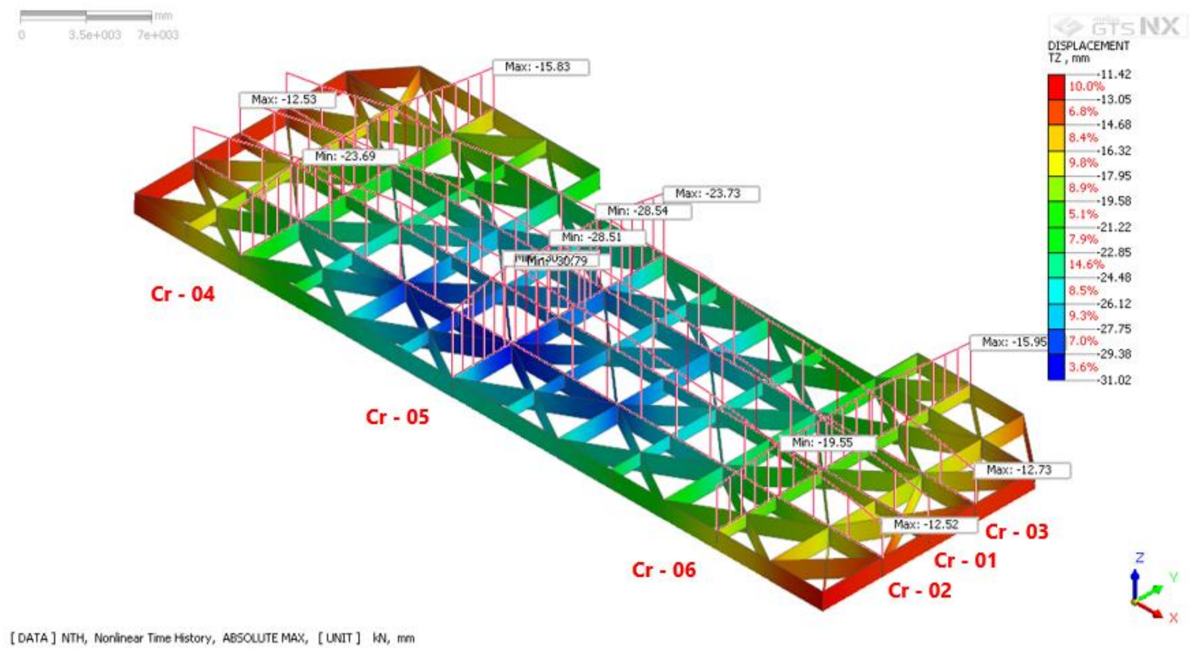

Figure 14. Displacement contour of KSLL foundation (dynamic condition)

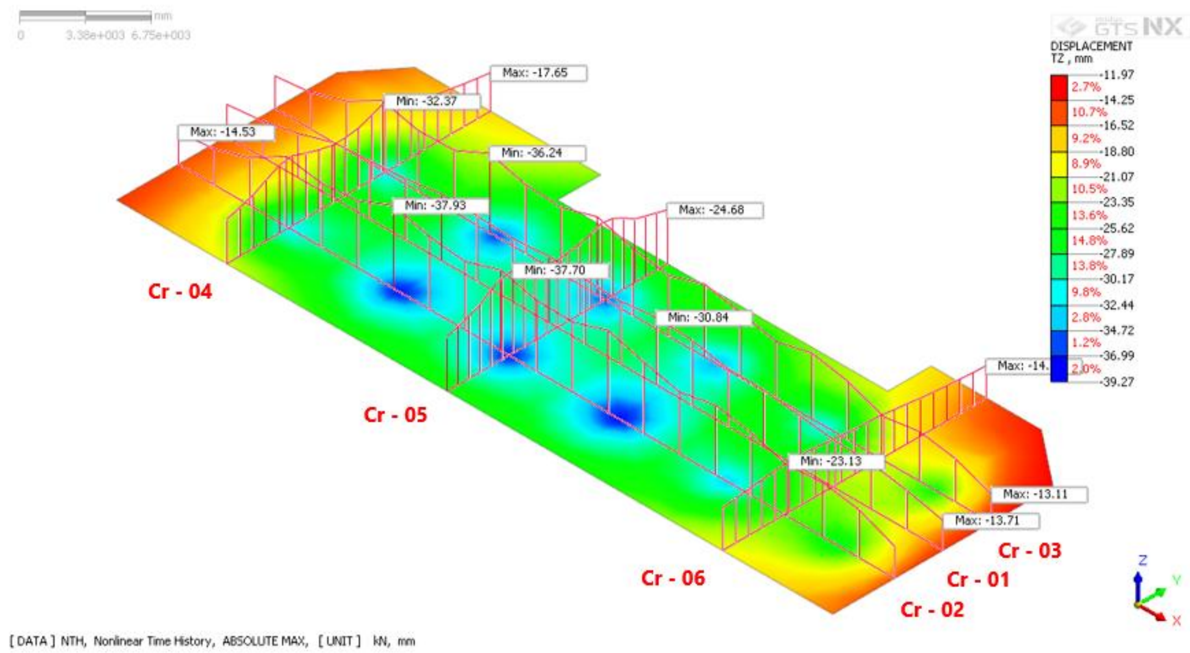

Figure 15. Displacement contour of raft foundation (dynamic condition)

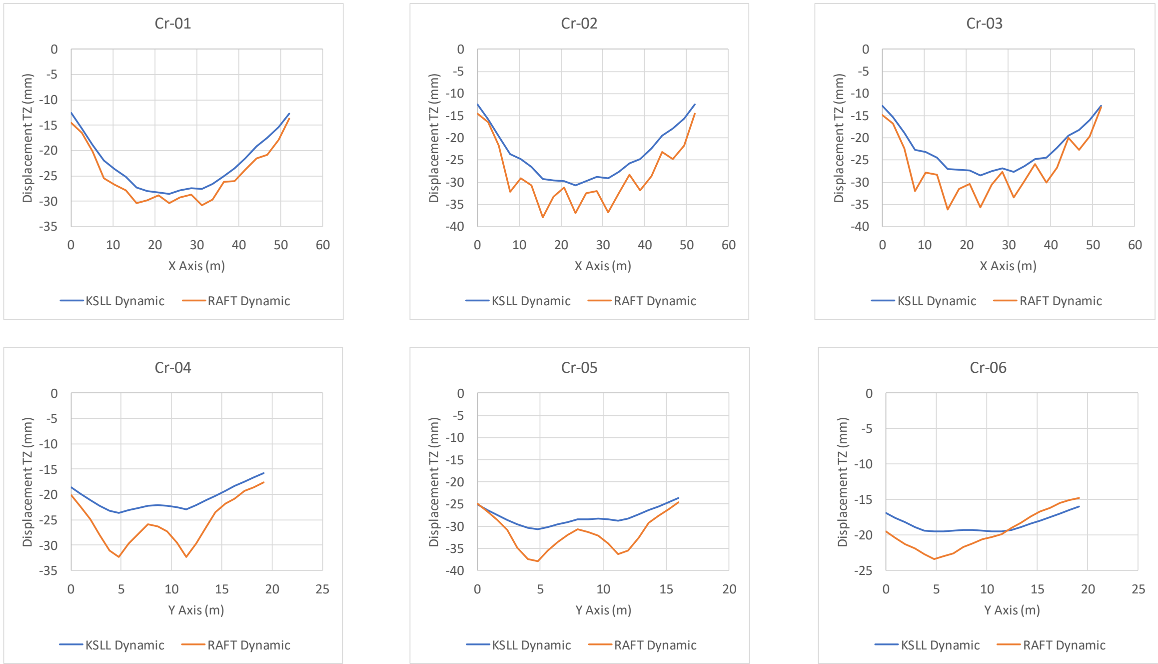

Figure 16. Displacement diagram of foundation (dynamic condition)

5.3 Internal Forces Result

In addition to settlement performance, the structural response of the foundations was evaluated based on the internal forces developed within the foundation elements. The principal internal forces considered in this study include axial force, bending moment, and shear force. Table 3 and Raft foundation *moment capacities (AS3600:2018): M*(+) = 245.8 kNm M*(-) = 326.9 kNm*
**Exceeds positive bending moment capacity (245.8 kNm)*
Table 4 summaries the maximum and minimum internal forces obtained from the static and dynamic analyses, respectively. Internal force components Force XX, Force YY, Moment XX, and Moment YY refer to the global coordinate system shown in Figure 7.

Under static loading conditions, the maximum positive bending moment developed in the equivalent raft foundation reached 319 kN.m, exceeding the estimated positive moment capacity of 245.8 kN.m. In contrast, the KSLL foundation developed significantly lower bending moments. Under dynamic loading conditions, the maximum raft bending moment remained below the estimated moment capacity. These results indicate that the 290 mm thick equivalent raft foundation is structurally inadequate under static loading despite having the same concrete volume as the KSLL foundation.

Table 3. Internal force result under static load

Type	Force XX (kN)		Force YY (kN)		Force XY (kN)		Moment XX (kN.m)		Moment YY (kN.m)		Moment XY (kN.m)		Shear XY (kN)		Shear YZ (kN)	
	Max	Min	Max	Min	Max	Min	Max	Min	Max	Min	Max	Min	Max	Min	Max	Min
KSLL	693	546	481	571	322	358	3	4	6	7	3	3	39	35	31	29
RAFT	84	189	53	208	94	67	319*	111	239	102	73	56	195	428	472	175

Raft foundation moment capacities (AS3600:2018): M(+) = 245.8 kNm M*(-) = 326.9 kNm*
**Exceeds positive bending moment capacity (245.8 kNm)*

Table 4. Internal force result under static load

Type	Force XX (kN)		Force YY (kN)		Force XY (kN)		Moment XX (kNm)		Moment YY (kNm)		Moment XY (kNm)		Shear XY (kN)		Shear YZ (kN)	
	Max	Min	Max	Min	Max	Min	Max	Min	Max	Min	Max	Min	Max	Min	Max	Min

KSLL	858	559	444	576	318	332	9	5	15	9	5	7	108	93	60	72
RAFT	277	356	260	186	87	156	178	79	176	85	45	37	367	243	181	276

Figure 17 shows the Force XY distributions obtained from the dynamic analysis. Compared with the equivalent raft foundation, the KSLL foundation develops substantially larger axial forces along the ribs. The force pattern indicates that the rib network actively participates in load redistribution and behaves as a three-dimensional load-transfer system. In contrast, the raft foundation exhibits considerably smaller axial forces, indicating that load transfer is primarily governed by plate action rather than axial resistance.

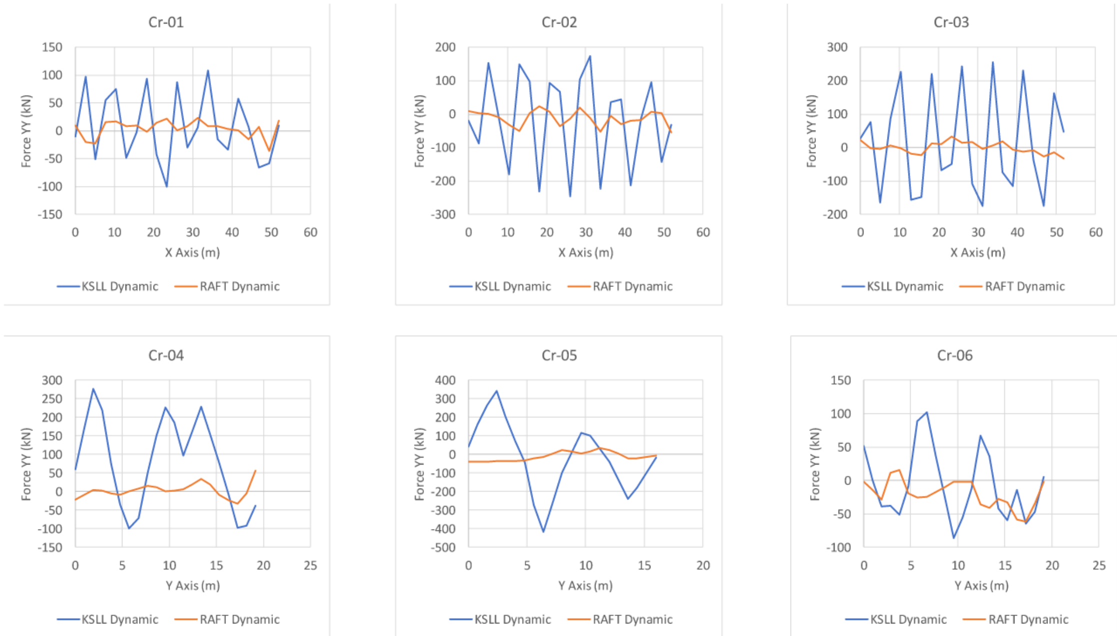

Figure 17. Representative force XY distributions under dynamic loading

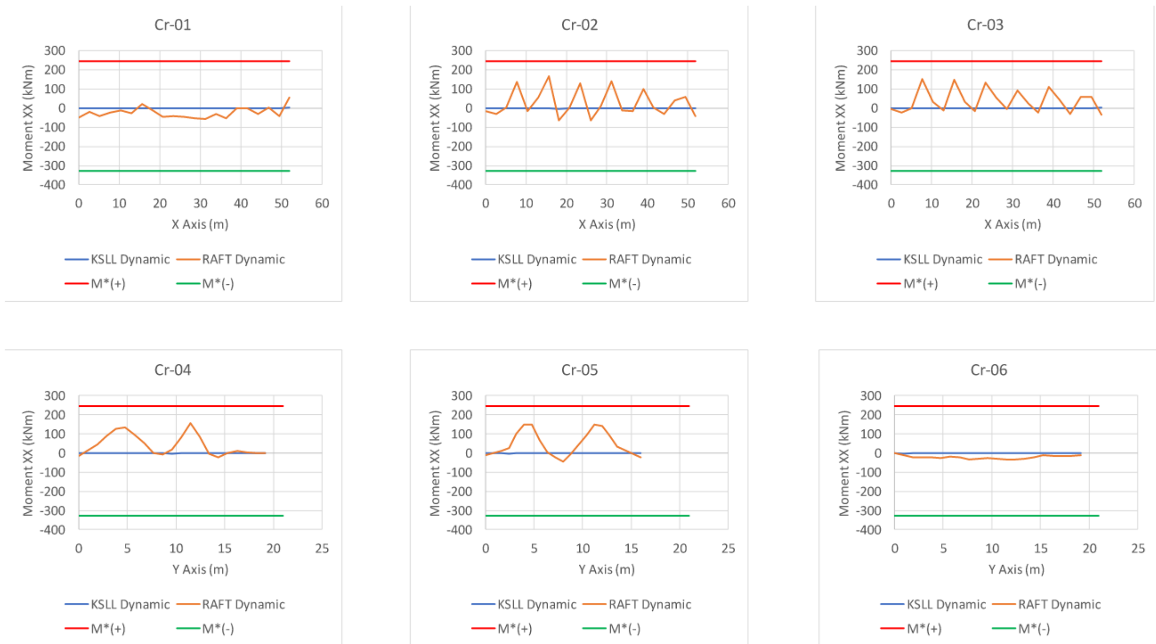

Figure 18. Representative moment XX distributions under dynamic loading

The bending moment distributions are shown in Figure 18. The KSLL foundation develops significantly smaller bending moments than the equivalent raft foundation throughout all representative sections. Under dynamic loading, the maximum Moment XX reaches approximately 9 kN.m in the KSLL foundation, whereas moments of up to 178 kN.m are observed in the equivalent raft foundation. Similar trends are observed for Moment YY and Moment XY. The lower bending demand in the KSLL foundation demonstrates that a substantial portion of the structural load is transferred through axial action within the ribs rather than through flexural resistance.

Although the KSLL foundation generates larger axial forces than the equivalent raft foundation, it develops significantly lower bending moments and shear forces under both static and dynamic loading conditions. This behaviour indicates a more efficient structural mechanism in which loads are distributed through the interconnected rib system rather than being resisted primarily by slab bending. Consequently, stress concentrations beneath the column locations are reduced, leading to a more uniform deformation pattern and improved structural performance compared with the equivalent raft foundation.

6 DISCUSSION

6.1 Settlement Behaviour Comparison

A comparison of settlement behavior shows that the KSLL foundation experiences significantly less deformation than an equivalent raft foundation, under both static and dynamic loading conditions. This difference indicates that the KSLL system has higher overall stiffness and better load-distribution capabilities.

Under static loading, the maximum settlement of the KSLL foundation is 43% less than the equivalent raft foundation (18.5 mm vs. 32.61 mm). This difference indicates that settlement behaviour is primarily governed by foundation stiffness and load-distribution efficiency, both of which are enhanced by the KSLL rib system.

Similarly, under dynamic loading, the KSLL foundation continues to exhibit lower settlement than the equivalent raft foundation, but at smaller gap (21% less at 31 mm vs. 39.3 mm). This reduction is attributed to the generation of excess pore water pressure within the liquefiable UBCSand layer, which reduces soil stiffness and contributes significantly to the overall deformation response. As both foundation systems are supported by the same liquefiable soil layer, a larger proportion of the total settlement under dynamic loading originates from soil deformation rather than foundation behaviour alone.

6.2 Load Transfer Mechanism

The structural configuration of the KSLL foundation transforms the load-transfer mechanism from a system dominated by bending, as seen in conventional raft foundations, into a three-dimensional load-distribution system in which axial forces along the ribs play a significant role. According to the full-scale static load test reported by Darjanto et al. (2015), load transfer in the KSLL foundation occurs progressively through several mechanisms. At relatively low loads, the load is primarily resisted by end bearing at the rib tips. As the applied load increases, load transfer is increasingly mobilized through shaft resistance along the rib-soil interfaces. Once the bearing and shaft resistances approach their limiting values, the load is further distributed through the slab and compacted soil fill, resulting in a composite soil-structure interaction system.

In raft foundations, loads are primarily transferred through the bending action of the slab. This flexure-dominated behavior often leads to stress concentrations beneath column loads and increases the risk of local punching deformation, especially when the slab thickness is insufficient.

In contrast, KSLL foundations consist of a rib system that forms a spatial structural framework. Vertical ribs act as stiffeners that significantly enhance structural stiffness. Load transfer occurs through a combination of axial forces along the ribs and plate membrane action, rather than solely through bending.

This mechanism is supported by the internal force results. Under static loading, the KSLL foundation develops maximum axial forces of 693 kN (Force XX) and 571 kN (Force YY), compared with 189 kN and 208 kN, respectively, for the raft foundation. However, the raft foundation develops substantially larger bending moments, with maximum values of 320 kN.m (Moment XX) and 239 kN.m (Moment YY), whereas the corresponding KSLL values are only 4 kN.m and 7 kN.m. Similar trends are observed under dynamic loading. These results suggest that the KSLL system transfers load primarily through axial action within the ribs, while the equivalent raft foundation relies predominantly on slab bending.

Additionally, the interaction between the ribs and the compacted soil fill contributes to soil-structure composite behavior. This interaction further increases stiffness and reduces stress concentration under column loads.

6.3 Structural Efficiency Using Equivalent Concrete Volume

When evaluated using the equivalent concrete volume approach, the KSLL foundation demonstrates higher structural efficiency compared to the raft foundation.

Although they have the same concrete volume, a 29-cm-thick raft foundation is structurally inadequate, as evidenced by positive bending moments that exceed its moment capacity under static loading conditions. This highlights the limitations of the raft system when constrained by material equivalence.

Additional sensitivity study analysis was carried out to find out the raft foundation thickness required to achieve comparable performance (result on Figure 19). Based on this analysis, a slab thickness of 80 cm is required, with an estimated increase in concrete volume of 2.5 to 3 times that of the KSLL foundation, to achieve deformation that is relatively distributed and not concentrated at the column locations.

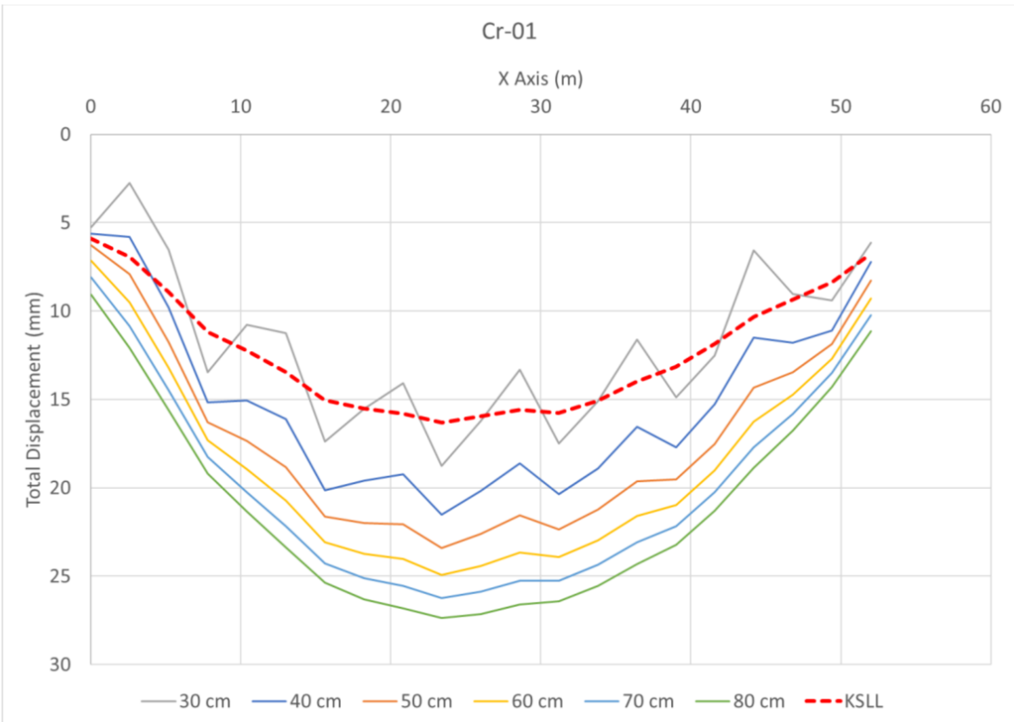

Figure 19. Displacement curve from sensitivity study of raft foundation thickness

These findings confirm that the KSLL foundation utilizes materials more efficiently by shifting the load transfer mechanism to a system dominated by axial forces, thereby reducing reliance on flexural resistance and minimizing structural demands.

6.4 Behaviour Under Liquefaction Conditions

Under conditions of soil liquefaction, the response of both foundation systems is influenced by excess pore water pressure generation and the associated reduction in soil stiffness within the liquefiable layer. Consequently, the governing mechanism of deformation shifts from foundation stiffness to soil behaviour.

Despite this change in governing mechanism, the KSLL foundation continues to exhibit lower settlement than the equivalent raft foundation under dynamic loading. The KSLL foundation utilizes a three-dimensional ribbed configuration that provides multiple load-transfer paths and promotes load redistribution through axial action. This results in larger axial forces but significantly lower bending moments and shear forces than the equivalent raft foundation, contributing to a more uniform deformation response.

Overall, the KSLL foundation demonstrates better deformation control than the equivalent raft foundation under both static and dynamic loading conditions. Although the performance gap decreases under dynamic loading due to liquefaction-induced soil softening, the KSLL foundation continues to exhibit lower settlement and a more uniform settlement profile.

7 CONCLUSION

This study presents a 3D-numerical analysis comparing the structural performance of KSLL foundations and conventional raft foundations under static and dynamic loads at sites prone to liquefaction. Based on the results, the following conclusions can be drawn:

1. The KSLL foundation exhibits significantly less settlement compared to an equivalent raft foundation, under both static and dynamic loading conditions. The maximum settlement of the KSLL foundation under static and dynamic loading is 18.5 mm and 31 mm respectively, whereas the equivalent raft foundation reaches 32.61 mm and 39.3 mm under static and dynamic loading respectively.
2. Internal force analysis indicates that the KSLL foundation transfers structural loads predominantly through axial action within the rib system. Although larger axial forces are developed, bending moments and shear forces remain substantially lower than those of the equivalent raft foundation. This load-transfer mechanism contributes to improved structural efficiency and reduced flexural demand under both static and dynamic loading conditions.
3. A raft foundation with a thickness of 29 cm experiences local punching deformation and generates bending moments exceeding its structural capacity. To achieve a deformation pattern comparable to that of the KSLL foundation, the raft foundation requires a much greater thickness, resulting in a concrete volume approximately of 2.5 to 3 times larger.
4. Under dynamic loading conditions representing seismic effects and potential liquefaction, the KSLL foundation maintains relatively stable deformation behavior. The three-dimensional ribbed configuration increases the global stiffness of the foundation system and enhances its ability to redistribute loads even when soil stiffness decreases due to excess pore water pressure.

Overall, the KSLL foundation demonstrates a more efficient structural mechanism and better deformation control compared to the conventional raft foundation when evaluated using an equivalent concrete volume approach. The ribbed configuration not only improves structural stiffness but also enhances soil–structure interaction behavior.

This study contributes to the understanding of the structural and geotechnical behavior of spider web (KSLL) foundation systems and highlights its potential advantages for structures located in seismic regions with liquefaction-prone soils.

ACKNOWLEDGEMENTS

The authors gratefully acknowledge Prof. Paulus P. Rahardjo and Dr. Martin Wijaya for providing access to project data, including the geotechnical investigation, foundation design information, and site-specific seismic hazard assessment for the University Hospital project in Jember. The data were used as the basis for the numerical analyses presented in this study.

DISCLAIMER

The authors declare no conflict of interest.

REFERENCES

Beaty & Byrne, 2011. UBCSAND Constitutive Model Version 904aR. Retrieved from: http://www.itasca-udm.com/media/download/UBCSand/UBCSAND_UDM_Documentation.pdf

Darjanto et al, 2015. Full Scale Static Load Test on The Spider Net System. *Malaysia: Jurnal Teknologi (Sciences & Engineering)*, 77(11), pp. 73-82. https://doi.org/10.11113/JT.V77.6424

Kementrian PUPR RI, 2019. Kumpulan Korelasi Parameter Geoteknik dan Fondasi. Jakarta.

PT Katama Suryabumi, 2011. KSLL (Konstruksi Sarang Laba-Laba). Accessed from: https://www.katama.co.id/services/ksll on 27 August 2022

Youd & Idriss, 2001. Liquefaction Resistance of Soils: Summary Report from the 1996 NCEER and 1998 NCEER/NSF Workshop on Evaluation of Liquefaction Resistance Soil. *Journal of Geotechnical and Geoenvironmental Engineering*, 127(4), pp. 297-313. https://doi.org/10.1061/(ASCE)1090-0241(2001)127:10(817)

USGS, 1999. The Ring of Fire. USA: United State Geological Survey (USGS). Accessed from: https://pubs.usgs.gov/publications/text/fire.html on: 27 Agustus 2022

- This page is intentionally left blank -